Boron Nitride Sputter Erosion Measurements by Cavity Ring-Down Spectroscopy

IEPC-2007-075

Presented at the 30th International Electric Propulsion Conference, Florence, Italy, September 17 –September 20, 2007

Azer P. Yalin*, Lei Tao†, Naoji Yamamoto‡
Colorado State University, Fort Collins, Colorado, 80523 USA

Timothy B. Smith§, Alec D. Gallimore**
University of Michigan, Ann Arbor, Michigan, 48109 USA

Abstract: Sputter erosion is a critically important process in many electric propulsion (EP) devices from the point of view of both lifetime assessment and contamination effects. In many Hall thrusters erosion of boron nitride (BN) is of primary interest. In this contribution we introduce the use of cavity ring-down spectroscopy (CRDS) as a diagnostic for measurement of sputtered BN. The measurement approach is based upon probing sputtered boron atoms in the region of 250 nm. We report proof of principle CRDS measurements of sputtered boron atoms from both boron and BN targets. The measurements are obtained with pulsed CRDS in a diagnostic chamber consisting of an ion beam incident on the target materials. We also outline the design of a higher sensitivity continuous-wave (cw) CRDS system using the fourth harmonic beam from an external cavity diode laser as the light source. The cw-CRDS system will be used for near real time sputter erosion measurements of thruster devices. Anticipated signal levels and signal-to-noise for the cw-CRDS system are discussed.

Nomenclature

A_{ki}	=	Einstein *A* coefficient, 1/s
Abs	=	Absorbance
c	=	Speed of light, 2.998 x 10^8 m/s
g_i	=	Degeneracy of state *i*
g_k	=	Degeneracy of state *k*
$k(\nu)$	=	Absorption coefficient, m^{-1}
l	=	Length of the ring-down cavity, m
N_i	=	Lower state concentration, m^{-3}
R	=	Mirror reflectivity
ROC	=	Mirror radius-of-curvature, m
$S(t,\nu)$	=	Ring-down signal
ν	=	Laser frequency, Hz
ν_{ki}	=	Transition frequency, 1/s
τ	=	Ring-down time, s
τ_0	=	Empty cavity ring-down time, s

I. Introduction

The Hall thruster is an electrostatic engine that was developed in the 1960s to alleviate the thrust density limitation of ion thrusters that results from space-charge effects within the acceleration volume. Hall thrusters were

* Assistant Professor, Mechanical Engineering, ayalin@engr.colostate.edu
† Graduate Student, Mechanical Engineering, leitao@lamar.colostate.edu
‡ Post-Doctoral Researcher, Mechanical Engineering, naojiya@engr.colostate.edu
§ Post-Doctoral Researcher, Aerospace Engineering, timsmith@umich.edu
** Professor, Aerospace Engineering, rasta@umich.edu

also attractive from the standpoint that since grids are not required to accelerate ions, they do not suffer from the large grid erosion rates of ion thrusters. Interest in the Hall thruster, though dormant in the U.S. from the early 1970s until the early 1990s, has seen a resurgence in recent years. Our focus is on the lifetimes of Hall thruster devices, especially stationary plasma thrusters (SPTs), for which sputter erosion of boron nitride (BN) from the acceleration channel is the primary life limiting factor. Despite the importance of BN erosion there is a lack of fundamental sputtering data on BN and a lack of available measurement techniques for *in situ* thruster studies. With proposed thrust durations now as long as 5-10+ years, ground-based life tests over the full thruster duration are becoming increasingly challenging. For example, an SPT-100 was operated for over 5,700 hours and performed nearly 7,000 start cycles at JPL as part of the engine's flight qualification process[1]. JPL also tested two ion thrusters continuously for 8,000 and 12,000 hours[2]. Clearly such approaches have numerous limitations including high cost and time intensiveness as well as only the possibility of *post-facto* bulk analysis as opposed to real time analysis as operating points are varied. Thus, it is necessary to develop advanced material diagnostics capable of circumventing such limitations.

The ideal diagnostic for *in situ* thruster studies should have high sensitivity to measure low erosion rates, the possibility of integration to a thruster test-facility, and fast time-response to explore a range of operating conditions. Techniques, such as weight loss[3], collector plates[4-5], quartz crystal microbalance[6-12], radioactive tracers[13], mass spectrometry[14], and Rutherford backscattering[15-16] each have certain advantages and can be appropriate for material sputter characterization studies, but none readily meets all of the above criteria. The need for a sensitive non-intrusive measurement suggests the use of optical techniques. Optical emission spectroscopy (OES)[17-18], laser induced fluorescence (LIF)[19-21], and multi-photon ionization coupled to a time of flight mass spectrometer[22-24] have all been used for species-specific sputtering measurements. The use of LIF has been particularly extensive, and has proven to be very effective for velocity measurement though challenging for quantitative number density. OES spectroscopy is attractive owing to its experimental simplicity but the analysis can be challenging since collisional-radiative modeling is required to extract number densities.

The approach presented here builds upon our previous development of cavity ring-down spectroscopy (CRDS) for sputtering measurements[25-29]. CRDS is a highly sensitive laser-based absorption method allowing species-specific measurement of concentrations of trace species. The technique is used extensively for trace-species measurement in flames, plasmas, and the atmosphere and we have developed its use for the study of sputtered particles in electric propulsion applications. Further discussion is provided in Section II.

In this contribution we present initial development of CRDS to study boron nitride. The approach is to detect sputtered boron atoms in the vicinity of 250 nm in the ultraviolet. CRDS measurements of boron present challenges owing to reduced mirror reflectivities in the ultraviolet. In order to achieve the required detection sensitivity we will implement CRDS with continuous-wave (cw) lasers for enhanced sensitivity. As a first step toward the cw-CRDS system we have performed proof of principle measurements of boron from both boron and BN targets using pulsed-CRDS in a diagnostic chamber which allows elevated boron number densities. In Section II of this paper we review the theory of CRDS and introduce the scheme for measuring BN. In Section III we present the proof of principle measurements of boron and BN targets. In Section IV we outline the design of the cw-CRDS system for device studies. Finally, a Summary is presented in Section V.

II. Cavity Ring-Down Spectroscopy (CRDS)

A. Technique Overview

CRDS is a highly sensitive laser-based absorption technique[30,31] that is directly quantifiable and thus well suited to measurements of low concentrations of sputtered particles. It is an absorption technique, so that unlike in fluorescence and emission, ground states are measurable. Measuring ground states can be advantageous since these levels typically contain a large fraction of the overall species population and their population fractions are less affected by collisional and radiative rates. The main practical impediment in applying CRDS is the need to study optically accessible species, i.e. to work at wavelengths where optical sources, detectors, and high-reflectivity mirrors are available. In terms of signal analysis, the path-integrated nature of CRDS can be challenging and may require the use of inversion (tomographic) techniques to recover spatially resolved profiles[29].

As shown in Fig. 1, the basic idea is to house the absorbing sample (i.e. the sputtered atoms) within a high-finesse optical cavity formed from high-reflectivity mirrors. The interrogating laser beam is coupled into the optical cavity where it "bounces" many times back-and-forth between the mirrors. Owing to the high reflectivity, the light within the cavity makes many passes within the cavity (e.g. ~10^4 passes for R~0.9999), and the effective path length and thus sensitivity is greatly increased. A detector placed behind the cavity measures the temporal decay of optical

intensity within the cavity. The difference in the temporal decay rate with and without the absorber (or with the laser tuned on/off the resonance) yields the sample concentration.

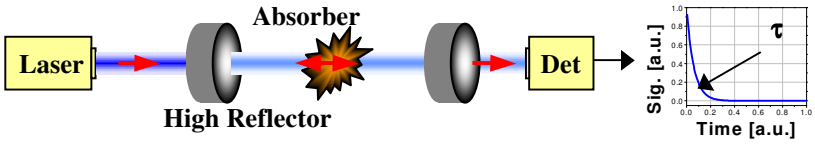

Figure 1. Schematic diagram of cavity ring-down spectroscopy (CRDS).

The technique affords high sensitivity owing to a combination of long effective path length and insensitivity to laser energy fluctuations (since a rate is measured). Under appropriate conditions, the ring-down signal $S(t,\nu)$ decays single exponentially[32,33] versus time as:

$$S(t,\nu) = S_0 \exp\left[-t/\tau(\nu)\right]$$
$$1/\tau(\nu) = \frac{c}{l}\left[\int k(x,\nu)dx + (1-R)\right] \quad (1)$$

where τ is the 1/e time of the decay (termed the ring-down time), c is the speed of light, l is the cavity length, $k(x,\nu)$ is the absorption coefficient, ν is the laser frequency, x is the position along the optical axis, and $1\text{-}R$ is the effective mirror loss (including scattering and all cavity losses). If the absorber is uniformly present over a column length l_{abs}, then $\int k(x,\nu)dx$ can be replaced with the product $k(\nu)l_{abs}$. In practice, the measured ring-down signal is fitted with an exponential, and the ring-down time τ is extracted. Combining τ with the "empty cavity ring-down time", τ_0 (which in practice is measured by detuning the laser) allows determination of the sample absorbance, Abs, and absorption coefficient:

$$Abs(\nu) \equiv \int k(x,\nu)dx = \frac{l}{c}\left[\frac{1}{\tau(\nu)} - \frac{1}{\tau_0}\right] \quad (2)$$

A commonly used approach is to scan the laser frequency across the absorption line and to measure the wavelength- (or frequency-) integrated spectrum (i.e. the line area). Assuming the spectroscopic line parameters are known, the measured area $\int Abs(\nu)d\nu$ of a transition from lower state i to upper state k can be readily converted to the path-integrated concentration of the lower state $\int N_i dx$ as:

$$\int N_i dx = 8\pi \frac{g_i}{g_k}\frac{\nu_{ki}^2}{A_{ki}c^2}\left(\int Abs(\nu)\,d\nu\right) \quad (3)$$

where g_i, g_k are the level degeneracies, ν_{ki} is the transition frequency, A_{ki} is the transition Einstein A coefficient, and c is the speed of light. For cases where the spatial distribution of particles is non-uniform, actual concentration profiles can be determined from the path-integrated concentration in several ways. For rough approximation one can assume a uniform concentration profile over a known column length, l_{abs}. Alternatively, Abel inversion or other inversion approaches based on inversion and modeled spatial profiles can be used[29]. CRDS can also be used to extract velocity information from the measured spectral lineshapes[28].

B. Boron Nitride Measurement Approach

Our approach for detection of boron nitride (BN) is based upon CRDS absorption measurement of sputtered boron atoms. (Atomic nitrogen is not a readily optically accessible species.) The exact composition of the sputtered particles, i.e. proportions of B, N, B_xN_y etc., is not well understood and may vary with sputtering conditions. However, at steady state, the composition of the sputtered particles must mimic the composition of the sputtered surface, and based on sputtering of other multi-component materials it is reasonable to expect a relatively high proportion of atomic boron amongst the sputtered particles. As a very rough start point we simply assume that each measured boron atom corresponds to ejection of one boron atom and one nitrogen atom from the BN surface though

this assumption will be refined. Assuming the composition is fixed then measured CRDS signals provide a sensitive and directly quantitative measure of the BN erosion.

Figure 2a shows a partial energy level diagram for non-ionizing resonance lines of neutral boron (B I), while Table 1 shows detailed energy levels, spontaneous emission rates (Einstein A coefficients), and wavelengths for the targeted lines. The ground term for this species has two distinct levels: $2s\ ^2P^0_{1/2}$ (at 0.00000 eV) and $2s\ ^2P^0_{3/2}$ (at 0.00189 eV). As a result, fine-structure splitting results in two distinct B I absorption lines near 250 nm: the $2s\ ^2P^0_{1/2} \rightarrow 3s\ ^2S_{1/2}$ absorption at 249.753 nm, and the $2s\ ^2P^0_{3/2} \rightarrow 3s\ ^2S_{1/2}$ absorption at 249.848 nm. The targeted lines are selected based on their optical accessibility and high absorption strength. The next lowest energy level is above 3 eV so that to a good approximation all population will reside in the split ground state, meaning that the measured states will provide a direct measure of the overall boron population. Figure 2b shows a simulated absorbance spectrum for the boron lines in the 249 nm region where we have assumed a boron number density of 10^8 cm^{-3} over a path length of 8 cm (corresponding to a path integrated concentration of $8x10^8$ cm^{-2}). At these conditions, the peak signals have optical absorbance of ~20 ppm. (For the linewidth in the simulated spectrum we use an estimated value based on our model for Doppler shifting and broadening developed in our velocity measurement work.)

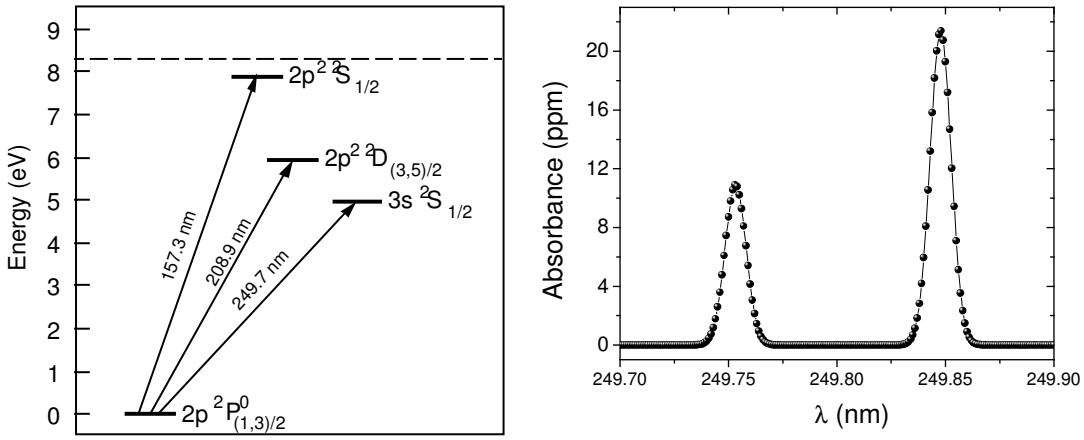

(a) Resonance lines of neutral boron. (b) Simulated absorbance spectrum.

Figure 2. Absorption lines and simulated CRD spectrum for neutral boron (from BN sputtering).

E_i (cm^{-1})	E_k (cm^{-1})	A_{ki} (s^{-1})	λ (nm)
0	40039.52	$9.552x10^7$	249.753
15.15	40039.52	$1.904x10^8$	249.848

Table 1. Spectroscopic information for boron (from NIST database).

III. Boron Measurement by Pulsed CRDS

A. Experimental Set-Up

Figure 3 shows a schematic diagram of the bench-top sputtering apparatus employed for CRDS diagnostic development[25]. The apparatus allows us to use CRDS to probe sputtered particles created by an ion beam incident upon a target. The key components are an ion beam and target, housed within a vacuum facility. A roughing and turbo-pump (Turbo-V550) are used to bring the pressure to approximately 10^{-6} torr under no-flow conditions. A small argon flow (1 sccm) is used to feed the system. The ion beam is extracted from an 8-cm diameter structurally integrated thruster obtained from NASA, and modified to operate on an inert gas, and to use refractory metal filaments for both the main and neutralizer cathodes in place of the hollow cathodes used in the original design. The beam is normally incident upon the target. The thruster operates with an IonTech power supply (MPS 3000), with

typical beam currents and voltages of about 10-100 mA, and 400-1200 V respectively. The ion beam is masked to an active area of 8 cm x 2.5 cm (with the 8 cm extent oriented parallel to the optical axis).

The CRDS set-up, schematically shown in Fig.3 uses a broadly tunable optical parametric oscillator (OPO) laser. For the boron experiments we use the doubled-signal beam as the light source in the 250 nm region. Laser parameters are: repetition rate = 10 Hz, pulse width ~ 7 ns, pulse energy ~ 2 mJ, and linewidth ~0.002 nm. We use a linear ring-down cavity of 75 cm length with 100 cm radius-of-curvature (ROC) mirrors (g=0.25). In order to prevent possible saturation effects, the laser energy is reduced with an attenuator to ~100 μJ/pulse prior to cavity injection. The ring-down signal is collected behind the output mirror with a fast photomultiplier tube (Hamamatsu R3896). Ring-down signals are fit between 90%-10% of the peak amplitude. We use area (frequency-integrated) measurements of absorbance in our analyses.

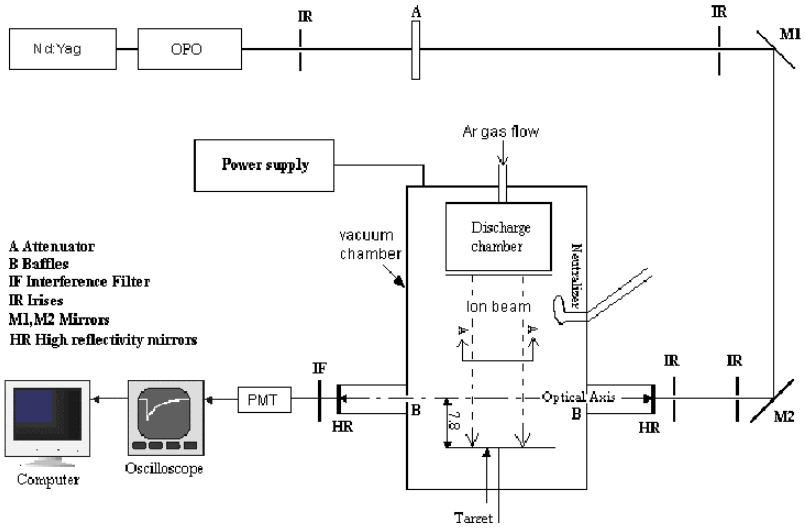

Figure 3. Schematic diagram of sputtering apparatus and CRDS system.

B. Pulsed CRD Spectra and Measurements

We have recently performed proof of principle experiments to detect boron using pulsed CRDS. Owing to the lower sensitivity of the pulsed version of the technique, we have operated our diagnostic chamber at sputtering conditions significantly higher than expected for a Hall thruster. The experimental configuration is as described above. A technical difficulty in the targeted wavelength region of ~250 nm is to obtain cavity mirrors with high reflectivity. While in the visible and infrared mirrors with dielectric coatings can have reflectivity above 0.9999, reflectivities tend to be lower in the ultra-violet (due to light absorption by the dielectric layers). The measurements described below used mirrors with R≈0.996 (corresponding to empty cavity ring-down times of approximately 0.65 μs for the 75 cm length cavity). The current upper limit on available reflectivity in this wavelength region appears to be a reflectivity of approximately 0.998, which would give approximately twice higher sensitivity than the current mirrors.

Prior to measuring boron nitride we have performed measurements from a boron sputtering target. The target is more than 99% pure and is circular with a diameter of 5.1 cm and was formed by hot-pressing. Ion beam conditions were a beam current of 45 mA and beam voltage of 1200 V and the optical axis was roughly 1 cm above the target. The left of Figure 4 shows the raw CRDS measurement for the 249.848 nm line. The wavelength step-size was 0.001 nm and at each wavelength step 48 ring-down signals are averaged (4.8 s per wavelength step). The right of Figure 4 shows the corresponding absorbance spectrum after baseline fitting and subtraction (eqn. (2) is used to convert ring-down times to absorbance values). Also shown in the right of Figure 4 is a best-fit Voigt peak. The absorbance spectrum is plotted in units of parts per million (referring to the absorbance not sample concentration). As discussed above, the area of the absorption peak (i.e. the wavelength- or frequency- integrated spectrum) is related to path-integrated concentration via eqn.(3). For the conditions of Figure 4 we find a path-integrated concentration of approximately $3x10^{10}$ cm^{-2}. For rough estimation we assume a uniform concentration over a path length of 5 cm corresponding to a concentration of ~$6x10^{9}$ cm^{-3}. These values are reasonable when scaled by current and voltage and compared with concentrations of other metals measured in our past research. For example,

we typically measure path-integrated concentrations of ~10^{10} cm^{-2} for beam currents of 20 mA and beam voltages of 750 eV.

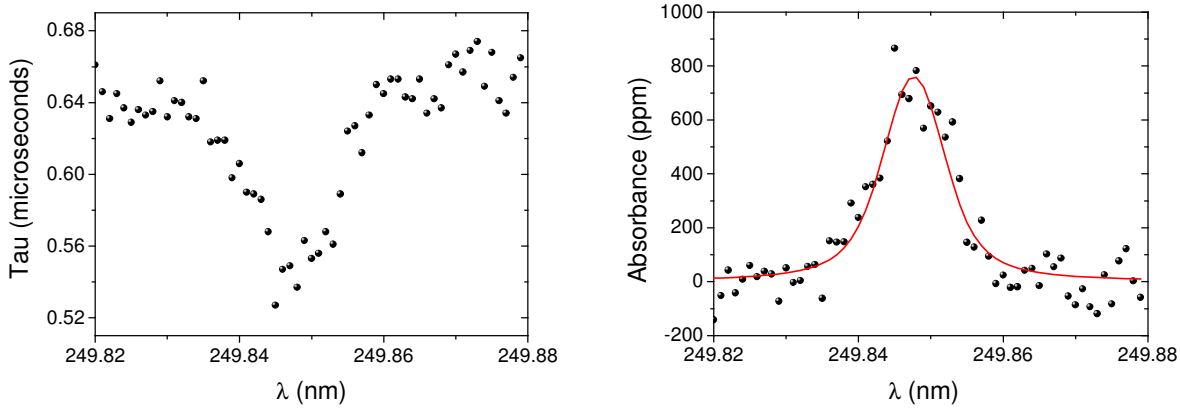

Figure 4. CRDS measurement of boron from boron target. Left: Raw data. Right: Absorbance spectrum.

Figure 5 shows initial measurements of sputtered boron atoms from boron nitride (BN) sputter erosion. The BN sample is HBC grade from General Electric's Advanced Ceramics and is formed by hot pressing. The target used was 10 cm by 10 cm. The left of Figure 5 shows the raw CRDS measurement for the 249.848 nm line. Ion beam conditions and data acquisition were as described above for the boron. The spectrum was obtained by scanning the laser from high to low wavelength and the baseline (empty cavity ring-down time) dropped during the measurement due to increased chamber heating causing slight misalignment. The right of Figure 5 shows the corresponding absorbance spectrum after baseline fitting and subtraction along with a best-fit Voigt peak. The absorbances are comparable to those for boron indicating a similar path-integrated concentration; however, the BN target is larger (and longer along the optical axis) so local concentrations may be lower. We also note that the spectral linewidth (full-width-half-maximum of the absorption feature) is narrower for the BN measurement as compared to the (pure) boron measurement. While we view this as a preliminary observation, it may be indicative of differences in the velocity profiles or differential sputter yield distributions in the two cases.

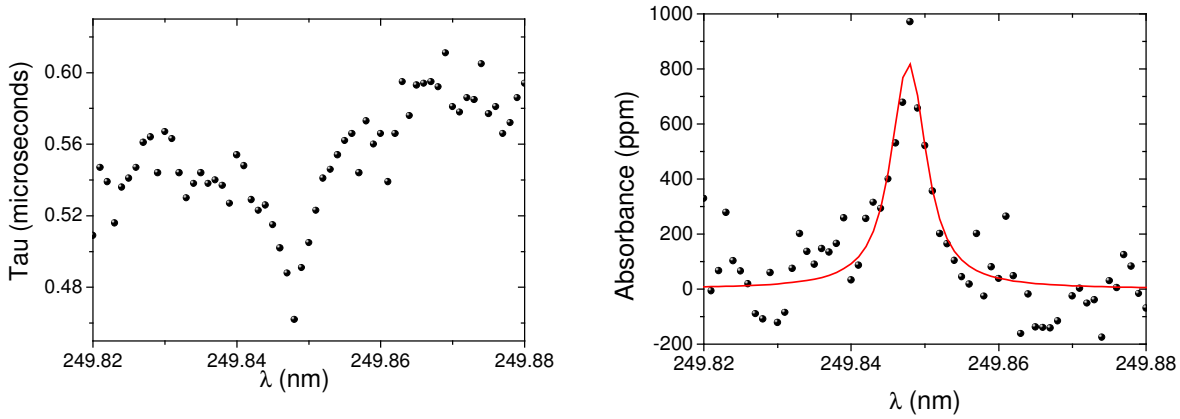

Figure 5. CRDS measurement of boron from BN target. Left: Raw data. Right: Absorbance spectrum.

Initial studies of dependence of boron number density versus beam current and beam voltage have been performed and are shown in Figure 6. The left of the figure is the current dependence and was obtained at constant beam voltage of 1000 V, while the right of the figure is the voltage dependence and was obtained at constant beam current of 60 mA. The number densities (concentrations) are determined as discussed above with areas of the absorption lines (and associated errors) found from Voigt fits to the data after baseline fitting and subtraction. The values are given as path-integrated number densities. For rough estimation of local number density a column length

of 10 cm (corresponding to the target dimension) can be assumed. At this voltage range one expects an approximately linear dependence on beam voltage (ion energy) as is observed. Similarly the concentration is expected to be proportional to the beam current, which is also as we observe. In this case the linear fit is constrained to pass through the origin.

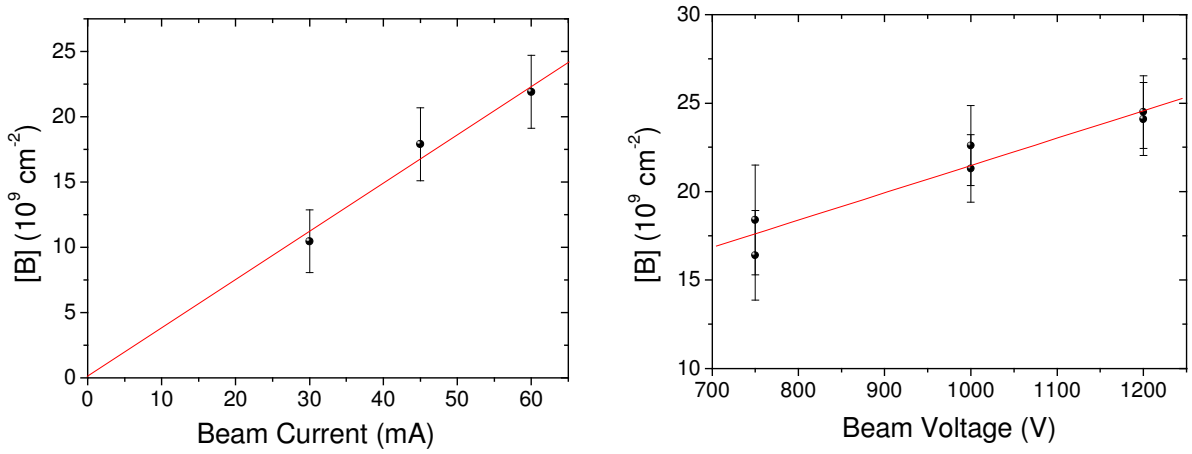

Figure 6. Left: Boron number density versus ion beam current. Right: Boron number density versus ion beam voltage.

IV. CW-CRDS System for Thruster Studies

A. Experimental Layout

A schematic diagram of the CRDS set-up that we propose for BN studies is shown in Figure 7. In this discussion, the emphasis is on the optical detection system that will be used in the diagnostic test-bed for initial diagnostic development and validation; the system for Hall thruster erosion studies will have similar optical design, with the major difference being the physical structure used to mount the cavity and optical components. Figure 8 shows a schematic diagram of the CRDS set-up for study of the plume of a Hall thruster. For improved sensitivity we employ cw-CRDS as opposed to pulsed-CRDS. The BN detection scheme is based on probing absorption lines in the vicinity of 249 nm as discussed above.

The cw-CRDS system will be based on a commercially available frequency-quadrupled external cavity diode laser as the illumination source. The external cavity diode laser has output of ~10 mW and offers narrow linewidth (~3 MHz) with continuous mode hop free tuning over ~15 GHz in our wavelength region of interest. The laser will be mode-matched to the cavity via several beam-shaping optics. The cavity will be based upon a pair of high-reflectivity mirrors (R>=0.996) at 250 nm. As described above, we will employ a ring-down cavity of length approximately 75 cm. The ring-down signals will be measured with a photo-detector (photomultiplier tube (PMT) or avalanche photodiode (APD)) and coupled to a computer using a custom data acquisition system. In order to precisely determine the wavelength axis, a simple reference leg will be used. A small portion of the laser beam will be picked-off and passed through a fused-silica etalon (with a free spectral range of 2 GHz. The etalon transmission peaks will be used for precise calibration of the wavelength axis.

In order to obtain exponential ring-down signals (as described by equation (1)) using the cw-CRDS system, one needs to appropriately control the laser and cavity frequencies. The basic issue is that the laser bandwidth (~3 MHz) is much narrower than the free-spectral range (i.e. the mode-spacing) of the ring-down cavity (FSR=$c/2l$=200 MHz for l=75 cm). Without some compensation, the laser wavelength will generally not coincide with a cavity-mode and will not be effectively transmitted through the cavity. (The analogous problem does not generally arise in pulsed CRDS measurements, since in that case the laser linewidth is generally not small compared to the cavity mode-spacing.) A multitude of approaches have been developed to address this issue for cw-CRDS and are discussed in the literature. We will employ a standard approach based on scanning the position of the rear cavity-mirror via a piezoelectric (PZT) stack and using an acousto-optic modulator (AOM) to extinguish the laser beam.

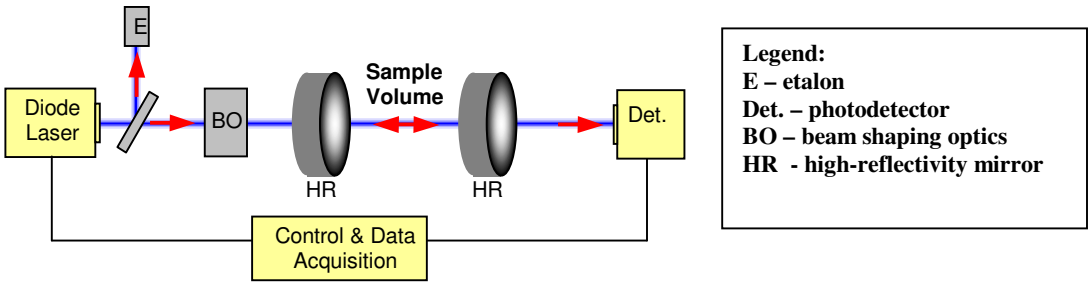

Figure 7. Schematic of cw-CRDS setup. (Piezoelectric transducer and acousto-optic modulator not shown.)

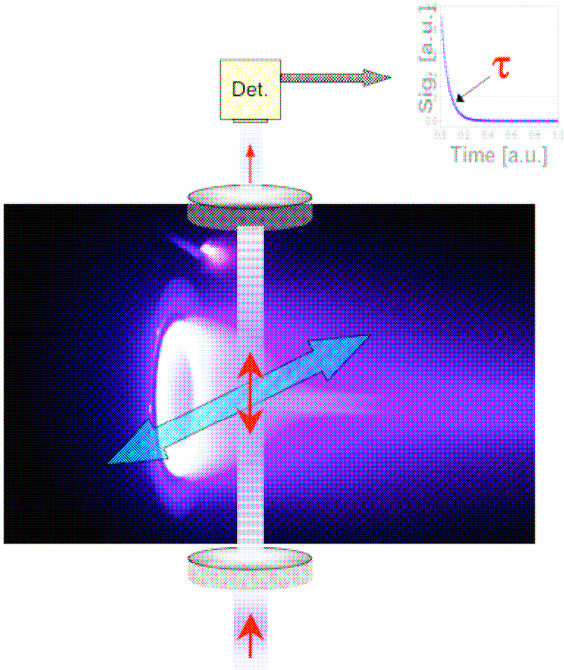

Figure 8. Schematic of integration of CRDS with the thruster.

B. Signal-to-Noise Estimation

The detection limit of our current (pulsed) CRDS system is ~50-100 ppm (though we have achieved ~2 ppm with higher reflectivity mirrors at other wavelengths) for measurement times of about 10s. Generally, the use of cw-CRDS (as opposed to pulsed CRDS) will improve detection limits by at least 100. Thus, we conservatively estimate that the detection limit of the proposed cw-CRDS system in the targeted wavelength region of ~250 nm will be an optical absorption ~0.5-1 ppm, corresponding to a path integrated number density of ~$3x10^7$ cm^{-2}. Increasing measurement times should allow further improvement in detection limit by a factor of approximately 10 (after which systematic errors may dominate).

To gauge our expected signal-to-noise ratio (SNR), we compare the anticipated detection limit with the expected value in the thruster plume. Based on scaling of wall erosion rates modeled by Yim et al.[34], we predict a path-integrated number density at the thruster exit plane of boron of 10^9 cm^{-2} to 10^{10} cm^{-2}. Thus, we anticipate that our CRDS detection system will allow sputter measurements with an SNR of 30 to 300. It is also interesting that (especially for long measurement times) the detection limit of our CRDS system is sufficiently low, that if the thruster tests do not yield a measurable signal, then we will have confirmed that the boron concentrations (~10^6 cm^{-3}) and associated erosion rates (~0.1 μm/hr) are low enough to correspond to very long thruster lifetimes (>9,000 hours). Although, as discussed above, CRDS is a self-calibrating technique, the diagnostic test-bed shown

in Figure 3 (with its well-characterized ion beam and simple target geometry) will allow us to confirm the relationship between the CRDS signals and boron concentrations.

V. Summary

We have presented number density measurements of boron atoms sputtered from both (pure) boron targets and from BN targets. The measurements employ laser-based CRDS in the region of 250 nm. Measurements in this spectral region are challenging owing to available mirror reflectivity. The measured number densities were in reasonable accord with expectations from modeling and past research. Dependence of sputtered particle number density on ion beam current and voltage was also measured and found to be in accord with expectations.

The boron measurements provide proof of principle for a BN erosion sensor that we will develop. The sensor will employ the cw-CRDS technique for further enhanced sensitivity. The cw-CRDS system will be initially implemented in the diagnostic test-bed chamber employed in this work, after which it will be integrated to a test facility at University of Michigan for thruster studies. Signal levels and signal to noise of the cw-CRDS sensor have been examined and should allow near real time measurements of sputter erosion in thruster devices, thereby providing a new and powerful tool for sputter erosion and lifetime studies.

Acknowledgments

The research was funded by Air Force Research Laboratory, Edwards Air Force Base.

References

[1] Garner, C. E., Brophy, J. R., Polk, J. E., and Pless, L. C., "A 5730-Hr Cyclic Endurance Test of the SPT-100," AIAA-95-2667, July, 1995.

[2] Anderson, J, Goodfellow, K., Polk, J., and Shotwell, H., "Results of an On-going Long Duration Ground Test of the DS-1 Flight Space Engine," AIAA-99-2858, 35th Joint Propulsion Conference, Los Angeles, CA July, 1999

[3]Yalin A. P., Surla V., Farnell C., Butweiller M., and Williams J. D. 2006 Sputtering studies of multi-component materials by weight loss and cavity ring-down spectroscopy, *42nd AIAA Joint Propulsion Conference* (Sacramento, CA)

[4]Chiplonkar V. T. and Rane S. R. 1965 Dependence of angular distribution of sputtering by positive ions from metal targets on the impact angle, *Indian J. Pure Appl Phys* 3 161

[5]Tsuge H. and Esho S. 1981 Angular distribution of sputtered atoms from polycrystalline metal targets, *J. Appl. Phys.* 52 4391-95

[6]Kolasinski R. D. 2005 Oblique angle sputtering yield measurements for ion thruster grid materials, *41st AIAA Joint Propulsion Conference* 2005-3526

[7]Kolasinksi R. D., Polk J. E., Goebel D. and Johnson L. J. 2006 Carbon sputtering yield measurements at grazing incidence, *42nd AIAA/ASME/SAE/ASEE Joint Propulsion Conference* (Sacramento, CA) *AIAA* 2006-4337

[8]Zoerb K. A., Williams J. D., Williams D. D., and Yalin A. P. 2005 Differential sputtering yields of refractory metals by xenon, krypton, and argon ion bombardment at normal and oblique incidences, *29th International Electric Propulsion Conference* (Princeton, NJ) IEPC-2005-293

[9]Yalin A. P., Williams J. D., Surla V., Wolf J., and Zoerb K. A. 2006 Azimuthal differential sputter yields of molybdenum by low energy ion bombardment, *42nd AIAA/ASME/SAE/ASEE Joint Propulsion Conference* (Sacramento, CA) 2006-4336

[10]Yalin A. P., Williams J. D., Surla V., and Zoerb K. A. 2007 Differential Sputter Yield Profiles of Molybdenum due to Bombardment by Low Energy Xenon Ions at Normal and Oblique Incidence, *Journal of Physics D – Applied Physics*

[11]Mannami M., Kimura K., and Kyoshima A. 1981 Angular distribution measurements of sputtered Au atoms with quartz oscillator microbalances, *Nuclear Instruments and Methods* 185 533-37

[12]Wickersham C. E. and Zhang Z 2005 Measurement of angular emission trajectories for magnetron-sputtered tantalum, *J. Electronic Materials* 34

[13]Kundu S., Ghose D., Basu D., and Karmohapatro S. B. 1985 The angular distribution of sputtered silver atoms, *Nuclear Instruments and Methods in Physics Research B* 12 352-57

[14]Wucher A. and Reuter W. 1988 Angular distribution of sputtered particles from metals and alloys, *J. Vac. Sci. Tech. A* 6(4) 2316-18

[15]Shutthanandan V., Ray P., Shivaparan N., Smith R., Thevuthasan T., and Mantenieks M. 1997 On the measurement of low-energy sputtering yield using Rutherford backscattering spectrometry, *25th International Electric Propulsion Conference* (Cleveland, OH) IEPC-97-069
[16]Mantenieks M., Foster J., Ray P., Shutthanandan S., and Thevuthasan T. 2001 Low energy xenon ion sputtering yield measurements, *27th International Electric Propulsion Conference* (Pasadena, CA) IEPC-01-309
[17]Andersen N., B. Andresen, and E. Veje 1982 Atomic excitations in sputtering processes, *Radiation Effects* 60 119-127
[18]Doerner R.P., Whyte D.G., and Goebel D.M. 2003 Sputtering yield measurements during low energy xenon plasma bombardment, *J. App. Phys.* 93(9) 5816-5823
[19] Pellin M.J., Wright R.B., and Gruen D.M. 1981 Laser fluorescence spectroscopy of sputtered zirconium atoms, *J. Chem. Phys.* 74 6448-6457
[20] Bay H.L. 1987 Laser induced fluorescence as a technique for investigations of sputtering phenomena, *Nuclear Instruments and Methods* B18 430-445
[21]Young C.E., *et al*.1984 Velocity and electronic state distributions of sputtered Fe atoms by laser-induced fluorescence spectroscopy, *J. Vac. Sci. Technol. A* 2(2) 693-697
[22]Nicolussi G., *et al*. 1995 Formation of metastable excited Ti and Ni atoms during sputtering, *Phys. Rev. B* 51(14) 8779-8788.
[23]Goehlich A. 2001 Investigation of time-of-flight and energy distributions of atoms and molecules sputtered from oxygen-covered metal surfaces by laser techniques, *Appl. Phys. A*. 72 523-529
[24]Staudt C., et al. 2002 Sputtering of Ag atoms into metastable excited states, *Phys. Rev. B* 66 085415 1-12
[25]Surla V., Wilbur P.J., Johnson M., Williams J.D., and Yalin A.P. 2004 Sputter erosion measurements of Titanium and Molybdenum by cavity ring-down spectroscopy, *Review of Scientific Instruments* 75(9) 3025-3030
[26]Yalin A.P., Surla V., Butweiller M., and Williams J.D. 2005 Detection of Sputtered Metals using Cavity Ring-Down Spectroscopy, *Applied Optics* 44, 30 6496-6505
[27]Yalin A.P., Surla V., Farnell C., Butweiller M., and Williams J.D. 2006 Sputtering Studies of Multi-Component Materials by Weight Loss and Cavity Ring-Down Spectroscopy, *42nd AIAA Joint Propulsion Conference* (Sacramento, CA) 2006-4338
[28]A.P. Yalin, V. Surla, 2005 Velocity Measurements by Cavity Ring-Down Spectroscopy, *Optics Letters*, 30, 3219
[29]Surla V. and Yalin A.P. 2007 Differential Sputter Yield Measurements using Cavity Ring-Down Spectroscopy *Applied Optics – accepted for publication*
[30]Busch, K.W., and Busch, M.A., "Cavity-Ringdown Spectroscopy," ACS Symposium Series, Vol. 720, 1999.
[31]Berden, G., Peeters, R., and G. Meijer, "Cavity Ring-Down Spectroscopy: Experimental Schemes and Applications," International Reviews in Physical Chemistry, Vol.19, No.4, p. 565-607, 2000.
[32]Zalicki, P. and Zare, R.N., "Cavity ring-down spectroscopy for quantitative absorption measurements," Journal of Chemical Physics, Vol. 102, No.7, p. 2708-17, 1995.
[33]Yalin, A.P., and Zare, R.N., "Effect of Laser Lineshape on the Quantitative Analysis of Cavity Ring-Down Signals," Laser Physics, Vol.12, No.8, p. 1065-1072, 2002.
[34]Yim, J.T., Keidar, M., and Boyd. I.D., "An investigation of factors involved in Hall thruster wall erosion modeling, AIAA-2006-4657, 42nd Joint Propulsion Conference, Sacramento, CA, Jul 2006.